1576 *KSME International Journal, Vol. 16 No. 12, pp. 1576~1582, 2002*

# Effects of Rotor Misalignment in Airgap on Dynamic Response of an Eccentric Rotor in BLDC Motor

**Tae-Jong Kim*, Kyung-Tae Kim, Sang-Moon Hwang, No-Gill Park, Shi-Bok Lee**
*School of Mechanical Engineering and Research Institute of Mechanical Technology, Pusan National University, Pusan 609-735, Korea*

Vibration of a BLDC motor is a coupled phenomenon between mechanical characteristics and magnetic origins which takes place through the motor airgap. When relative misalignment of a rotor in the airgap is introduced during assembly, the dynamic characteristics of the motor system are affected. The rotor-motor system used in a washing machine is modeled using FETM and magnetic forces in a BLDC motor with radial rotor eccentricity are determined analytically. The transient whirl responses of a rotor system supported on two roller bearings with relative misalignment in the motor airgap are investigated by considering mechanical and magnetic coupling effects. Results show that rotor misalignment in the airgap considerably affects the vibration of the rotor-motor system.

**Key Words:** Eccentric Rotor, Rotor Misalignment, Magnetic Unbalanced Forces, Dynamic Response

## 1. Introduction

The drive motor is often the most important element in many precision motor applications and also a frequent source of the vibration and acoustic noise. In the previous research works reported in open literature, vibrations of mechanically and magnetically induced sources have been treated separately (Subbiah and Kumar, 1988; Kumar and Sankar, 1986; Kim and Lieu, 1998; Jang and Lieu, 1996). However, these two origins are coupled in nature (Kim et al., 2000; Yoon et al., 1997).

The differences between dynamic effects in hydrodynamically lubricated bearings and in rolling-element bearings can be expressed as differences in spring constants and damping coefficients. Roller bearings have lower damping capacity than hydrodynamic bearings and the latter also exhibits nonlinear stiffness effects. Compared with hydrodynamic conformal sliding bearings, more severe alignment requirements are needed for rolling bearings. The roller bearing mounts must be carefully aligned for colinearity and angularity to avoid creating excessive vibration levels in the bearings during assembly. It is important to investigate the dynamic response of an eccentric rotor supported on roller bearings to estimate its reliability and to reduce vibration and noise levels. A relative parallel misalignment in the airgap can be formed by biased bearings during assembly. It can greatly influence the dynamic characteristics of rotor systems depending on the degree of airgap misalignment. Rotor misalignment and other mechanically unbalanced forces induce cylindrical and conical whirl of the rotor-bearing system and the rotor whirl causes the variation of the air-gap, thus yielding the net magnetic unbalanced forces acting on the rotor, which again adversely affect the whirl of the rotor-motor system.

This paper presents a magnetic force analysis of brushless DC (BLDC) motors with radial eccen-

* Corresponding Author,
**E-mail**: tjong@puson.ac.kr
**TEL**: +82-51-510-2474; **FAX**: +82-51-514-7640
School of Mechanical Engineering and Research Institute of Mechanical Technology, Pusan National University, Pusan 609-735, Korea. (Manuscript **Received** October 15, 2001; **Revised** September 25, 2002)

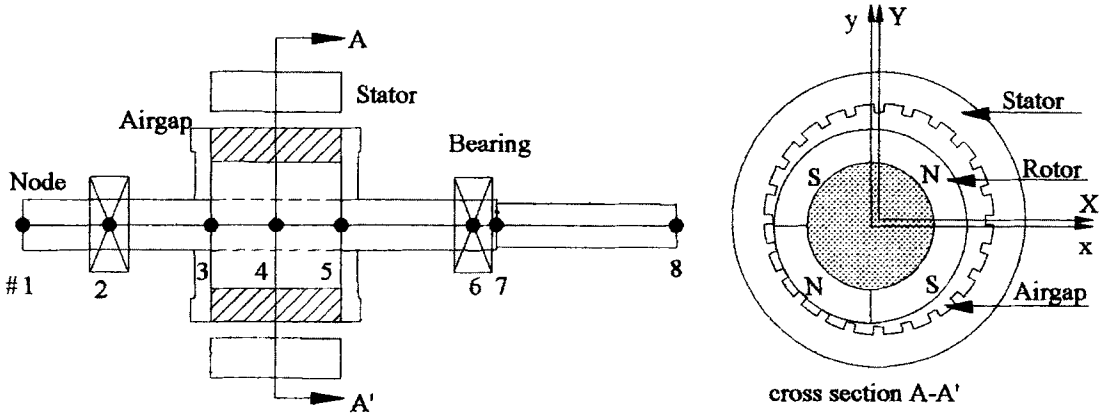


**Fig. 1** Rotor-motor system configuration

tricity due to rotor misalignment by using the perturbation method. The rotor-motor system in a washing machine is modeled by using the finite element transfer matrix (FETM) and the transient whirl responses for various rotor misalignment are determined by incorporating the mechanical and magnetic coupling.

## 2. Rotor Dynamics

The flexible rotor-bearing system shown in Fig. 1 consists of a shaft composed of rotor segments with distributed mass and elasticity, and discrete bearings. Each element is assumed to be continuous in diameter and the discontinuity in diameter is allowed only between elements. The end points of an element are called nodes, and they are located such that each bearing of the rotor coincides with a node. Dynamic behavior of the rotor system is influenced by the mass unbalance forces, reaction forces of roller bearings, and magnetic unbalanced forces.

The equation of motion for the finite shaft element $j$ with nodes $i$ and $i+1$ illustrated in Fig. 2 can be expressed in the $XYZ$ coordinates as

$$[M^s]\{\ddot{q}(t)\}+[C^s]\{\dot{q}(t)\}+[K^s]\{q(t)\} =\{F^s(t)\} \quad (1)$$

The bearings obey the governing equations of the form in the fixed frame coordinates given by

$$[C^b]\{\dot{q}(t)\}+[K^b]\{q(t)\}=\{F^b(t)\} \quad (2)$$

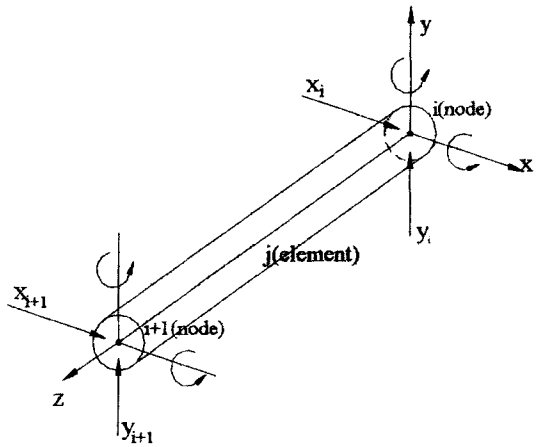


**Fig. 2** Finite element coordinates

By combining Eqs. (1) and (2), the assembled element system equation of motion for the element $j$ with nodes $i$ and $i+1$, can be expressed in the $XYZ$ coordinates as

$$[M_j]\{\ddot{q}(t)\}+[C_j]\{\dot{q}(t)\}+[K_j]\{q(t)\} =\{F(t)\} \quad (3)$$

where $\{F(t)\}=\{{}^{R}f_i(t)\,|\,{}^{L}f_{i+1}(t)\}^T$ are the generalized force vectors acting on nodes $i$ and $i+1$, and $\{q(t)\}=\{q_i(t)\,|\,q_{i+1}(t)\}=\{x_i\ y_i\ \beta_i\ \alpha_i\,|\,x_{i+1}\ y_{i+1}\ \beta_{i+1}\ \alpha_{i+1}\}^T$ are the generalized coordinates. Superscripts $R$ and $L$ represent right-and left-side elements, respectively, of the i-th node. Also, $[M_j]$, $[C_j]$, $[K_j]$ are the mass, damping and stiffness matrices of the element $j$, which can be expsessed by the following matrix partitions.

$$[M_j]=\begin{bmatrix}(m_{11})_j & (m_{12})_j\\ (m_{21})_j & (m_{22})_j\end{bmatrix}$$
$$[C_j]=\begin{bmatrix}(c_{11})_j & (c_{12})_j\\ (c_{21})_j & (c_{22})_j\end{bmatrix} \quad (4)$$
$$[K_j]=\begin{bmatrix}(k_{11})_j & (k_{12})_j\\ (k_{21})_j & (k_{22})_j\end{bmatrix}$$

Assuming a numerical scheme for differentials $\ddot{q}_i(t)$ and $\dot{q}_i(t)$, it can be shown that

$$\begin{aligned}\ddot{q}_i(t+\Delta t)&=A(t)\,q_i(t+\Delta t)+B_i(t)\\ \dot{q}_i(t+\Delta t)&=D(t)\,q_i(t+\Delta t)+E_i(t)\end{aligned} \quad (5)$$

where the coefficient $A(t)$, $B_i(t)$, $D(t)$ and $E_i(t)$ are all functions of the system properties at time $t$(Kumar and Sankar, 1986).

By merging Eq. (5) into Eq. (3), the following expression can be obtained.

$$\begin{bmatrix}(K_{11})_j & (K_{12})_j & (v_1)_j\\ (K_{21})_j & (K_{22})_j & (v_2)_j\\ 0 & 0 & 1\end{bmatrix}\begin{pmatrix}q_i(t)\\ q_{i+1}(t)\\ 1\end{pmatrix}=\begin{pmatrix}{}^{R}f_i(t)\\ {}^{L}f_{i+1}(t)\\ 1\end{pmatrix} \quad (6)$$

where,

$$\begin{aligned}(K_{11})_j&=A(t)\cdot(m_{11})_j+D(t)\cdot(m_{11})_j+(k_{11})_j\\ (K_{12})_j&=A(t)\cdot(m_{12})_j+D(t)\cdot(m_{12})_j+(k_{12})_j\\ (K_{21})_j&=A(t)\cdot(m_{21})_j+D(t)\cdot(m_{21})_j+(k_{21})_j\\ (K_{22})_j&=A(t)\cdot(m_{22})_j+D(t)\cdot(m_{22})_j+(k_{22})_j\\ (v_1)_j&=(m_{11})_j\cdot\{B_i(t)\}+(m_{12})_j\cdot\{B_{i+1}(t)\}\\ &\quad+(c_{11})_j\cdot\{E_i(t)\}+(c_{12})_j\cdot\{E_{i+1}(t)\}\\ (v_2)_j&=(m_{21})_j\cdot\{B_i(t)\}+(m_{22})_j\cdot\{B_{i+1}(t)\}\\ &\quad+(c_{21})_j\cdot\{E_i(t)\}+(c_{22})_j\cdot\{E_{i+1}(t)\}\end{aligned}$$

The unknown forces ${}^{R}f_i(t)$ and ${}^{L}f_i(t)$ at i-th node are related to the known external nodal force by

$${}^{R}f_i(t)+{}^{L}f_i(t)=f_i^{ext}(t) \quad (7)$$

If Eqs. (3) and (5) are used in conjunction with successive transformations, equation (3) can be rewritten as

$$U_{i+1}^{L}(t+\Delta t)=[T_j(t)]\cdot U_i^{L}(t+\Delta t) \quad (8)$$

where $U_i^{L}(t)=\{q_i(t)\ {}^{L}f_i(t)\ 1\}^{T}$, and $[T_j(t)]$ is the transfer matrix associated with j-th element. Recursive application of (8) gives the following relation

$$\begin{aligned}U_{n+1}^{L}(t+\Delta t)=&[T_n(t)]\cdot[T_{n-1}(t)]\\ &\cdots[T_1(t)]\cdot U_1^{L}(t+\Delta t)\end{aligned} \quad (9)$$

The boundary conditions at two end stations are applied as follows

$$\begin{aligned}{}^{L}f_1(t+\Delta t)&=0\\ {}^{L}f_{n+1}(t+\Delta t)&=f_{n+1}^{ext}(t+\Delta t)\end{aligned} \quad (10)$$

## 3. Magnetic Forces

The magnetic field equation in permanent magnet BLDC motor is given by

$$\begin{aligned}\frac{\partial^2\Phi_1}{\partial\xi^2}+\frac{1}{\xi}\frac{\partial\Phi_1}{\partial\xi}+\frac{1}{\xi_2}\frac{\partial^2\Phi_1}{\partial\psi^2}&=0\\ \frac{\partial^2\Phi_2}{\partial\xi^2}+\frac{1}{\xi}\frac{\partial\Phi_2}{\partial\xi}+\frac{1}{\xi^2}\frac{\partial^2\Phi_2}{\partial\psi^2}&=\frac{1}{\mu_r}\frac{M_\xi}{\xi}\end{aligned} \quad (11)$$

Using the perturbation method with appropriate boundary conditions, magnetic flux density can be found by the previous work (Kim and Lieu, 1998). For a 4-pole, 24-slot BLDC motor in Fig. 1 with geometric parameters in Table 1, the analytic radial magnetic flux density is shown in Fig. 3 with the eccentricity ratio (eccentricity/airgap length) of 0.5 and compared with FEM results. The discrepancy at slotting area and pole transition come from the error in prediction of permeance function and the first order approxi-

**Table 1** Geometric parameters of the motor

| Parameters | Symbol | Value(unit) |
|---|---|---|
| Airgap length | $g$ | 0.0006(m) |
| Radius of rotor | $R_m$ | 0.0344(m) |
| Pole pair | $p$ | 2 |
| Magnetic residual flux density | $B_r$ | 0.4(T) |
| Pole-arc/pole-pitch ratio | $a_p$ | 1 |
| Relative permeability of PM | $\mu_r$ | 1.061 |

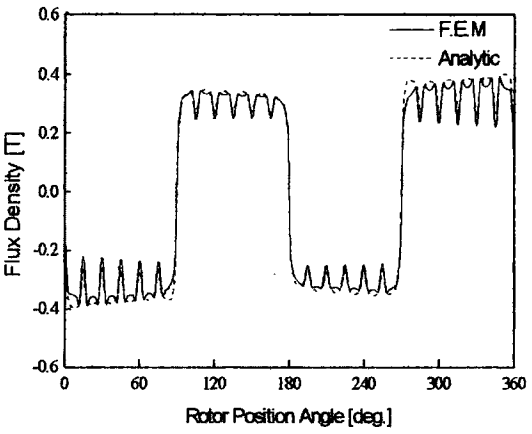


**Fig. 3** Radial magnetic flux density distribution

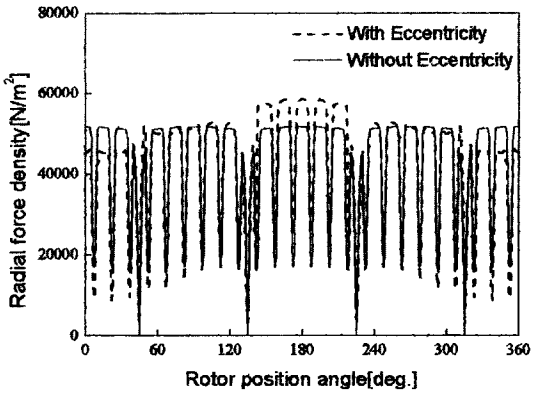


**Fig. 4** Radial local traction

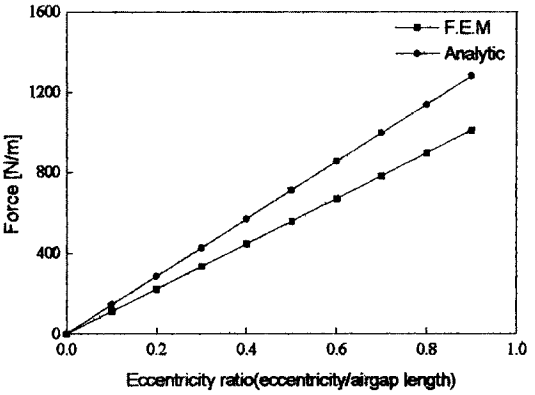


**Fig. 5** Unbalanced magnetic force

mation used in the perturbation method. The local traction forces acting on the rotor can be determined by using Maxwell stress tensor and given by

$$f_r=\frac{1}{2\mu_o}(B_r^2-B_\theta^2)$$
$$f_\theta=\frac{1}{\mu_o}B_rB_\theta \tag{12}$$

where $f_r$ and $f_\theta$ denote the radial and tangential local traction force components. Using the Cartesian coordinates, the corresponding traction force components are given as

$$f_x=f_r\cdot\cos\theta-f_\theta\cdot\sin\theta$$
$$f_y=f_r\cdot\sin\theta+f_\theta\cdot\cos\theta \tag{13}$$

Figure 4 shows the radial local traction force acting on the rotor surface without and with the eccentricity ratio of 0.5. With the rotor eccentricity, it can be seen that the radial local traction force is stronger in the narrow airgap region. It can be also seen that the symmetry of the radial local traction force is destroyed yielding net unbalanced magnetic force. The magnetic unbalanced forces acting on the rotor center can be determined by integrating the corresponding local traction forces over the rotor surface and are given by

$$F_{x,mag}=\int_0^{2\pi}f_x\cdot r\cdot d\theta$$
$$F_{y,mag}=\int_0^{2\pi}f_y\cdot r\cdot d\theta \tag{14}$$

Figure 5 shows the maximum magnitude of the unbalanced magnetic forces with respect to various rotor eccentricities. It should be noted that the increased discrepancy between the analytic and FEM results mainly comes from the first order approximation of the perturbation method with increased rotor eccentricity. The mechanical and magnetic coupling effects can be clearly observed as the rotor eccentricity or rotor misalignment is increased. Since the magnetic forces are nearly proportional to the rotor eccentricity, they can be simplified as

$$F_{x,mag}=A\cdot\varepsilon\cdot\cos(\omega t+\phi)$$
$$F_{y,mag}=A\cdot\varepsilon\cdot\sin(\omega t+\phi) \tag{15}$$

where $A$ , $\phi$ and $\varepsilon$ are a constant, the angle of eccentricity and the eccentricity of the rotor, respectively. Noting that the magnetic forces in Eq. (15) can be expressed with the generalized displacement $\{q(t)\}$, they can be transferred to the left side of Eq. (3), thus reducing the system stiffness. It is predicted that the reduced system stiffness generally enhances the dynamic responses of the system.

## 4. Dynamic Response

A vertical type rotor-bearing system to be analyzed consists of a rotor with 7 finite segments and 2 roller bearings, as shown in Fig. 1. The data for this rotor system is listed in Table 2. Excitation forces on the rotor system include the mass unbalance forces, reaction forces of roller

**Table 2** Rotor configuration data

| Element Number | Mass(g) | Length(mm) | Radius(mm) |
|---|---|---|---|
| 1 | 0.041 | 30 | 7.5 |
| 2 | 0.042 | 30.5 | 7.5 |
| 3 | 0.499 | 19.5 | 34.4 |
| 4 | 0.499 | 19.5 | 34.4 |
| 5 | 0.054 | 39.5 | 7.5 |
| 6 | 0.1 | 7 | 7.5 |
| 7 | 0.065 | 54 | 7.0 |

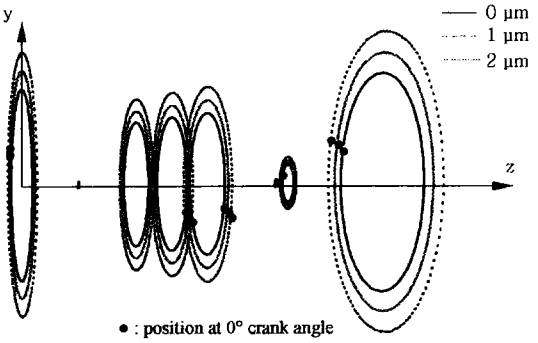


**Fig. 6** Steady state orbits along the rotor axis with respect to the rotor misalignment

bearings, and magnetic unbalanced forces. For rotor dynamics, the 2 roller bearings have the same stiffness of $K_{XX}=K_{YY}=1.0\times10^9$ N/m. The shaft has a modulus of elasticity $E_S=1.6\times10^{11}$ N/m$^2$ and for the motor rotor, $E_m=1.2\times10^{11}$ N/m$^2$. The mass unbalances of the rotor section at element number 3 and 4 are assumed to be located at stations #3 and #5 with the same magnitude. The magnitude of the unbalance is varied between $m_{u3}=m_{u5}=75$ mg, 150 mg, 300 mg, while $r_{u3}=r_{u5}=27.5$ mm and $\phi_{u3}=0°$, $\phi_{u5}=180°$. The rotational speed was held constant at 10,000 rpm, and the time step size was set at $5\times10^{-5}$ seconds.

The FETM was applied to the rotor-motor system to illustrate the misalignment effect in rotor dynamics. The dynamic response of a rotor with magnetic forces can be obtained with respect to relative misalignment in the airgap. The steady state orbits at nodes along the rotor axis for various rotor misalignment values are shown in Fig. 6, where both the mechanical and magnetic coupling effects taken into account. Figure 7 shows a converging transient orbit at the rotor

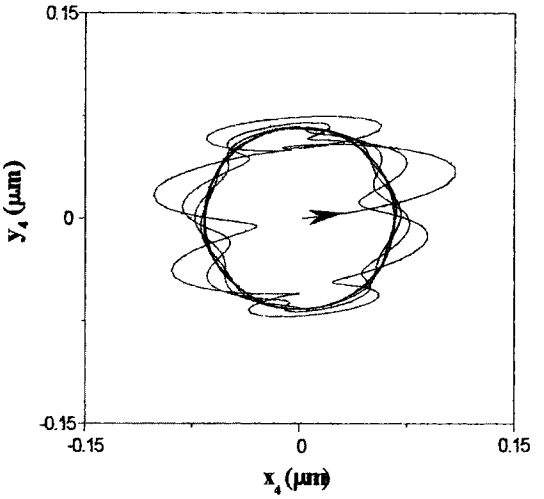


**Fig. 7** Converging transient orbit at rotor center without misalignment

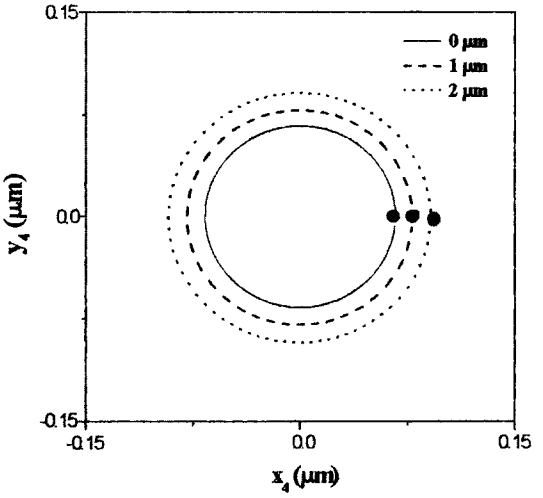


**Fig. 8** Comparison for orbits at rotor center for various misalignment values with $m_{u3}=m_{u5}=75$ mg

center calculated for 5 cycles without the rotor misalignment. Figure 8 shows a comparison of steady state orbit responses in microns with respect to the rotor misalignment given the unbalance magnitude of $m_{u3}=m_{um}=75$ mg. Figure 9 shows a comparison of orbits at the rotor center station with respect to the mass unbalance without the misalignment. Also, Fig. 10 shows a comparison of orbits at the rotor center station with respect to the mass unbalance given a 2 $\mu$m

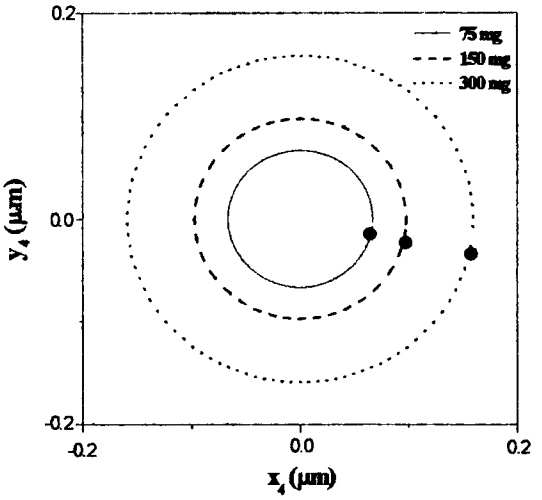


**Fig. 9** Comparison of orbits at rotor center with respect to mass unbalance without misalignment

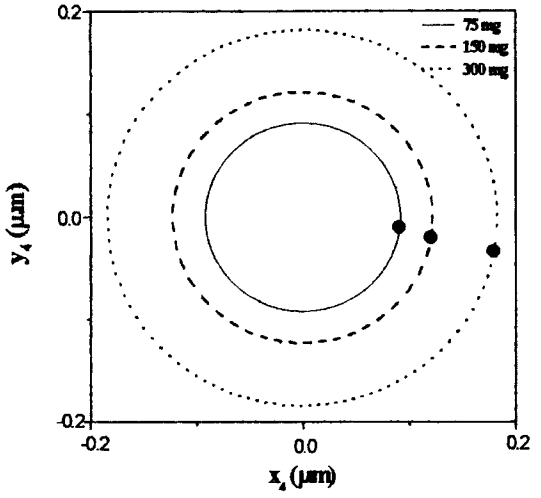


**Fig. 10** Comparison of orbits at rotor center for various mass unbalance values with 2 μm misalignment

misalignment. With the existence of magnetic forces, the mechanical and magnetic coupling effects while considering a misalignment phenomenon are incorporated into the system equations of motion. With increased misalignment, the whirl magnitudes of the rotor is also increased due to increased unbalanced magnetic forces as shown in Fig. 11 which reduce the system stiffness. Figure 8 shows a comparison of steady

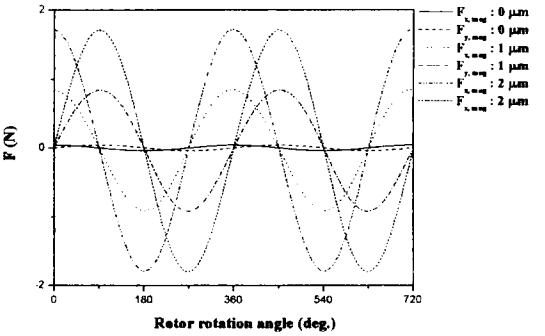


**Fig. 11** Unbalanced magnetic forces for various misalignment values

state orbit responses for various rotor misalignment values. It can be seen that the whirl magnitude with a 1-micron misalignment at x- and y-directions is increased by 17.7 percent compared to that without the misalignment. Also, the whirl magnitude with a 2-micron misalignment in x-, y- directions is increased by 36.9 percent compared to that without the misalignment. Therefore, the rotor misalignment coupled with unbalanced magnetic forces adversely affects the dynamic characteristic of the rotor-motor system supported on roller bearings.

## 5. Conclusion

The FETM method was applied to a rotor-motor system to illustrate the effect of misalignment on rotor dynamics. The dynamic response of a rotor with magnetic forces can be obtained by varying the degree of misalignment in the airgap. The steady state orbits at nodes along the rotor axis without any misalignment is obtained by considering the mechanical and magnetic coupling effects. The transient orbits of the rotating shaft without the rotor misalignments show a stable whirl condition compared to the rotor with misalignment present. With increased misalignment, the whirl magnitudes of the rotor are also increased due to increased unbalanced magnetic force that acts to reduce the system stiffness. This is because the unbalanced magnetic forces act as external forces in the airgap of the stator. Therefore, a rotor misalignment coupled with unbalanced magnetic forces adversely affects the

dynamic characteristic of the rotor-motor system.

## References

Jang Gunhee and Lieu, Dennis K., 1996, "Analysis of the Magnetic Force and the Torque in a Brushless DC Motor," *KSME International Journal*, Vol. 10, No. 1, pp. 37~48.

Kim Tae-Jong, Hwang Sang-Moon and Park No-Gill, 2000, "Analysis of Vibration for Permanent Magnet Motors Considering Mechanical and Magnetic Coupling Effects," *IEEE Transactions on Magnetics*, Vol. 36, No. 4, pp. 1346~1350.

Kim Ungtae and Lieu, Dennis K., 1998, "Magnetic Field Calculation in Permanent Magnet Motors with Rotor Eccentricity: With Slotting Effect Considered," *IEEE Trans. Mag.* Vol. 29, pp. 2253~2266.

Kumar, A. S. and Sankar, T. S., 1986, "A New Transfer Matrix Method for Response Analysis of Large Dynamic Systems," *Computers & Structures*, Vol. 23, No. 4, pp. 545~552.

Subbiah, R. and Kumar, A. S., 1988, "Transient Dynamic Analysis of Rotors Using the Combined Methodologies of Finite Elements and Transfer Matrix," *Journal of Applied Mechanics, Trans. ASME*, Vol. 55, pp. 448~452.

Yoon Yeo-Kwon, Jeong Ho-Seop and Lee Chong-Won, 1997, "Compensation of Tool Axis Misalignment in Active Magnetic Bearing Spindle System" *KSME International Journal*, Vol. 11, No. 2, pp. 155~163.